

Structural Model Construction and Optimal Characterization of High-Volatile Bituminous Coal Molecules

Deji Jing,* Xiangxi Meng,*[†] Shaocheng Ge, Tian Zhang, Mingxing Ma, and Gang WangCite This: *ACS Omega* 2022, 7, 18350–18360

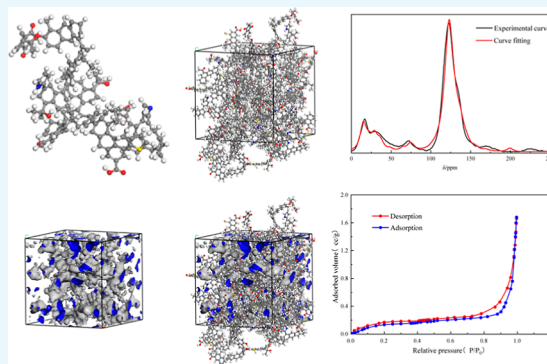
Read Online

ACCESS |

Metrics & More

Article Recommendations

ABSTRACT: The structural characteristics of coal at the molecular level are important for its efficient use. Bituminous coal from the Baozigou Coal Mine is investigated, using elemental analysis, ¹³C nuclear magnetic resonance, X-ray photoelectron spectroscopy, and Fourier transform infrared. The molecular structure was determined. The aromatic compounds of bituminous coal molecules are primarily two- and three-ring structures, and the aliphatic structures are primarily in the form of methyl, ethyl side chains, and naphthenic hydrocarbons. The ratio of aromatic bridge carbon to peripheral carbon in the molecular structure is 0.279. Oxygen atoms in the form of carbonyl, phenolic hydroxyl and C–O, and nitrogen atoms in pyrroles. Thus, the average structure model of bituminous coal macromolecules was constructed; the molecular formula was C₁₆₉H₁₂₈O₁₀N₂S, and the molecular weight was 2378. The aromatic structural units in the macromolecular structure of coal include four naphthalenes, three anthracenes, two tetracenes, and heteroatoms in the form of three carbonyl groups, one phenolic hydroxyl group, one pyrrole, and one pyridine. The structure optimization and annealing kinetic simulation of a single macromolecular structure model were performed. Chemical bonds such as bridge bonds and aliphatic bonds were found to be twisted, and π – π interactions between the aromatic sheets in the molecule produced adjacent aromatic sheets. This arrangement tends to be approximately parallel, and the total energy decreases from 6713.401 to 2667.595 kJ/mol, among which the bond stretching energy and van der Waals energy dominate. We used 20 bituminous coal macromolecular models to construct aggregated structural models. After optimization by molecular dynamics simulation, the macromolecules were constrained by the surrounding molecules, and the sheet-like aromatic carbon structures that were originally approximately parallel were distorted. The macromolecular structure model of bituminous coal constructed in this study provides a theoretical model basis for the optimal surfactant.



1. INTRODUCTION

With the improvement of coal mine production systems, coal dust pollution remains one of the five major factors contributing to coal mine disasters.^{1–3} Particularly, in various mining working faces,^{4–6} the production of coal dust in the efficient production process of coal mines can seriously endanger the health of miners,^{7,8} and the accumulation and diffusion of coal dust concentrations seriously endanger normal production underground work.^{9–11} Pneumoconiosis can occur after exposure to a high-concentration coal dust operation environment over the long term.¹² Suppressing dust production at its source has always been a difficult problem. However, the physical properties of coal dust are hydrophobic, and increasing the contact between the solution and coal dust is an important factor in inhibiting its release and diffusion. Accelerating the contact efficiency of the solution and coal dust can effectively improve the underground working and production environment.^{13–15} To effectively improve the production environment of each mining face, we investigate the bituminous coal from the Baozigou Coal Mine, Shanxi Province, and use various spectral

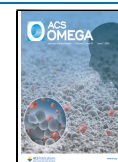
analyses to determine coal structure parameters, establish its structure, and the properties of bituminous coal at the molecular level.^{16–18}

Ping et al.¹⁹ used a combination of X-ray photoelectron spectroscopy (XPS), ¹³C nuclear magnetic resonance (NMR), and Fourier transform infrared (FT-IR) to establish three-dimensional (3D) molecular models of vitrinite and inertite, whose molecular formulas are C₁₂₆H₉₉O₁₂N₃S₂ and C₁₃₁H₉₈O₁₇, respectively, the predicted spectra demonstrate that these models are able to reflect the true molecular structure of coal. Lin et al.²⁰ established structural models of raw coal, ldi and hdi from ¹³C NMR, FT-IR, and XPS. The characterization data and

Received: January 25, 2022

Accepted: May 12, 2022

Published: May 23, 2022



molecular structure model showed no significant difference in the aromaticity. The structural units of all the samples were nearly identical. Wang et al.²¹ used ¹³C NMR and FT-IR to construct small molecular structures of different coal samples and analyzed the evolution process of different coal qualities. He et al.²² analyzed the chemical structures of metamorphic coals with different grades from lignite to anthracite using FT-IR and ¹³C NMR, and concluded that the evolution structure of coal is complex and has three stages, with $R_o = 0.4\text{--}1.3$, $1.3\text{--}2.0$, and $2.0\text{--}4.0\%$, respectively. When $R_o = 0.4\text{--}1.3\%$, the rapid decline of oxygen-containing functional groups accompanied by enrichment is the main feature of aliphatic compounds. Currently, scholars have proposed more than 130 average structure models of coal molecules through research on the coal structure, and the most commonly used structural models are Fuchs, Given, Wisner, and Shinn. These models can explain the swelling, cracking, gas adsorption, and flotation behavior of coal to some extent. Using FT-IR and image processing techniques on coal structures, the image distribution is analyzed to determine the size and distribution of aromatic fused rings and combined with other testing and analysis techniques to construct ideal coal molecule structural models.^{23–26}

Bituminous coal from the Baozigou Coal Mine is investigated in this study using industrial analysis, elemental analysis, ¹³C NMR, FT-IR, and XPS. The molecular structure was studied by various means, and the average molecular structure model was constructed accordingly.^{27–30} The structure was optimized by the kinetic optimization algorithm in the Forcite module of Materials Studio software,^{31–33} and the optimization model was simulated by annealing dynamics.^{34–36} To use a molecular dynamics simulation to study the evolution of the crystallite structure of the coal at the molecular scale, the evolution of the crystallite structure provides a basis for the model,^{37–39} and the pore volume of the Baozigou bituminous coal is given.

2. EXPERIMENTAL MATERIALS AND METHODOLOGY

2.1. Experimental Coal Samples. Experimental coal samples were selected from bituminous coal from the 10,103

Table 1. Element Analysis of the Baozigou Coal Industry

density (g/cm ³)	element content analysis %				
	C %	H %	O %	N %	S %
1.3	81.3	4	9.89	1.12	3.69

working face of the Baozigou Coal Industry Company (the density of coal is 1.3 g/cm³). The national standard GB/T 482–2008 was selected from the #9 coal seam for sampling. Coal samples with marked defects were eliminated, and intact coal samples were ground into 200 minus in the laboratory. The samples were placed in a constant-temperature oven at 80 °C for continuous drying for 24 h, and then the coal samples were subjected to coal analysis, NMR experiments, XPS experiments, and FT-IR.

2.2. Elemental Composition. To construct the molecular structure model of the Baozigou Coal Mine, the elemental industrial analysis of Baozigou coal samples was performed using a German Allimonta unicube element analyzer, and the element contents of C, H, N, and S were determined. The O content was calculated by the subtraction method, and the results of industrial element analysis are shown in Table 1.

2.3. FT-IR Experiment. FT-IR was performed using the KBr pellet method. The raw ore sample and KBr powder were weighed and mixed at a ratio of 1:200, fully ground in an agate mortar, pressed into a transparent sheet with a thickness of approximately 0.5 mm, and dried in an oven at 110 °C for 6 h.⁴⁰ The FT-IR test was completed using a Nicolet6700 FT-IR spectrometer that was produced by Thermo Fisher Company in the United States, with a resolution of 4 cm⁻¹, accumulative scanning times of 32 times, and a measured spectral range of 400–4000 cm⁻¹.

Spectral analysis can be performed to determine which compounds or functional groups exist in the sample. With a clear absorption peak position, the content of these compounds or functional groups can also be quantitatively analyzed. The absorption peaks in the IR spectrum of coal can be divided into four types: (1) aromatic structures with absorption peaks at 900–700 cm⁻¹; (2) =C stretching vibration and –CH₃, –CH₂ deformation vibration, and other structures; (3) the absorption peak is located in the fat structure of 3000–2800 cm⁻¹; and (4) the absorption peak is located in the hydroxyl structure of 3000–3600 cm⁻¹.

2.4. ¹³C NMR Experiment. The solid-state C spectrum analysis used a Bruker AVANCE III HD 400 MHz solid-state NMR spectrometer and a H/X dual-resonance solid-state probe with a 4 mm ZrO₂ rotor as the benchmark. The rotational speed was 5 kHz, and the detection resonance frequency of ¹³C was 100.625 MHz. The sampling time was 5.12 μs, the spectral width was 50 kHz, and the loop delay time was 6.5 μs.

2.5. XPS Experiment. The coal samples were tested using an X-ray photoelectron spectrometer (Thermo Fisher, ESCALAB Xi+, USA). The pressure of the analysis chamber reached 8 × 10⁻¹⁰ Pa, the excitation source was Al Kα ray ($h\nu = 1486.6$ eV), the working voltage was 12.5 kV, the filament current was 16 mA, and the signal accumulation occurred over 10 cycles. The full passing energy spectrum was 100 eV, the narrow spectrum was 30 eV, the step size of each step was 0.05 eV, the residence time of the test was 40–50 ms, and charge correction was performed with a binding energy of C1 s = 284.80 eV as the energy standard. Finally, the C1 s, O1 s, N1 s, and S2 p nuclear magnetic spectra of the carbon spectrum were tested in the form of data.

2.6. Low Temperature Nitrogen Adsorption Experiment. The nitrogen adsorption experiment was completed using the JW-ZQ200 cryogenic liquid nitrogen adsorption instrument. The samples were ground, crushed, and screened to 200 minus. 2 g of samples were taken, dried in a drying box at a constant temperature of 60 °C for 24 h, and vacuum degassed for 24 h. During the adsorption experiment, the saturation pressure was maintained at 77.35 K, liquid nitrogen with a purity of more than 99.999% was used as the adsorbate, and the adsorption experiment was carried out at a relative pressure of 0.01–0.995.

2.7. Molecular Dynamics Simulation Method. To determine the lowest energy configuration of the single-molecule structure model, geometry optimization and annealing kinetic simulation of the single-molecule structure model of bituminous coal were performed using Materials Studio software. The molecular structure of bituminous coal was imported into Materials Studio software, and its structure was saturated and hydrogenated. The geometric optimization of the simulation adopts the Forcite module, and the Smart Minimizer method was used for optimization. The parameters are set as follows: the Coulomb energy and van der Waals energy were

calculated based on the total energy of the atom. The net charge of the atom was obtained by the charge balance method, the number of iteration steps was 5000 steps, and the convergence criterion was fine. After geometry optimization, high-temperature relaxation was continued with the anneal of the Forcite module. The simulation process was performed under the *NVT* ensemble, and the Nosé temperature control method was selected. The initial temperature was set to 298 K, and the maximum temperature was set to 898 K. The heating rate was 50 K/time, and the simulation time was 200 ps.

Using the amorphous cell module in Materials Studio software, 20 optimized bituminous coal molecules were randomly added into a unit cell with a size of $36.4 \times 36.4 \times 36.4 \text{ \AA}^3$, and 3D periodic boundary conditions were added. The density of the structural model was set to 1.3 g/cm^3 , and the system was first relaxed by a geometric optimization molecular dynamics simulation, followed by an annealing kinetic simulation with the temperature set at 298~898 K and the final temperature kept at 298 K. The configuration system with the lowest energy was selected as the structure model of bituminous coal molecular aggregates under periodic boundary conditions.

3. RESULTS AND DISCUSSION

3.1. FT-IR Analysis. **3.1.1. Hydroxyl Absorption Peak.** Hydroxyl groups in coal primarily exist in the end groups and

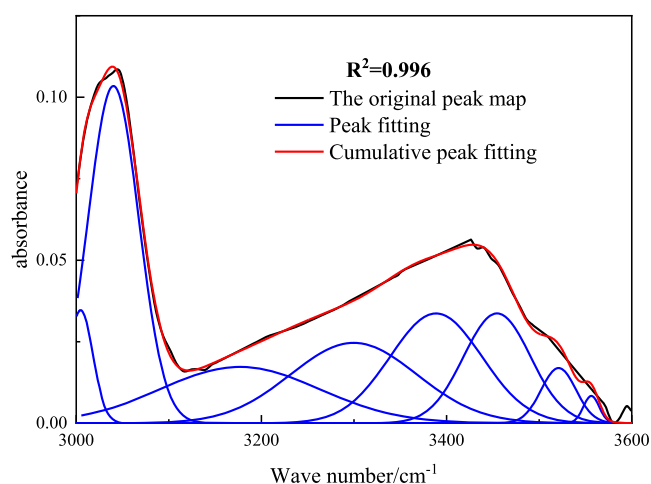


Figure 1. Hydroxyl FT-IR fitting spectrum.

side chains, which are important factors for the formation of hydrogen bonds in coal, generally determining the reaction properties of coal. Hydroxyls have a strong activation effect when breaking and cross-linking bonds. There are eight characteristic peaks in the FT-IR fitting spectrum of hydroxyl groups in Baozigou coal, as shown in Figure 1 ($R^2 = 0.996$). The specific absorption location data results are shown in Table 2.

According to Table 2,²² there is a hydroxyl absorption peak near the 3450 cm^{-1} absorption peak position. The hydroxyl groups in coal are generally hydrogen bonded, and the spectral peak position shifts from 3300 cm^{-1} , where the general hydroxyl group appears, to 3450 cm^{-1} . With increasing the coalification degree, the absorption peak gradually weakened, indicating that the number of hydroxyl groups decreased. At 3030 cm^{-1} , it is the absorption peak of aromatic hydrogen, and the intensity of the peak reflects the degree of polycondensation of the aromatic nucleus of the coal structure. The hydrogen bond with the

Table 2. FT-IR Analysis Table of Hydroxyl Groups in Coal

spectral position attribution	peak type	peak weighted center (cm^{-1})	fwhm	peak area	peak area percentage (%)
aromatic hydrogen	Gaussian	3004.82	31.30	0.73	3.14
aromatic hydrogen	Gaussian	3040.19	64.62	6.59	28.18
aromatic hydrogen	Gaussian	3176.76	202.25	3.64	15.56
aromatic hydrogen	Gaussian	3299.71	160.72	4.22	18.01
—OH	Gaussian	3388.61	116.86	4.19	17.89
hydrogen bonded —OH	Gaussian	3454.54	85.19	3.06	13.05
hydrogen bonded —OH	Gaussian	3521.01	44.28	0.79	3.41
hydrogen bonded —OH	Gaussian	3556.28	20.01	0.18	0.76

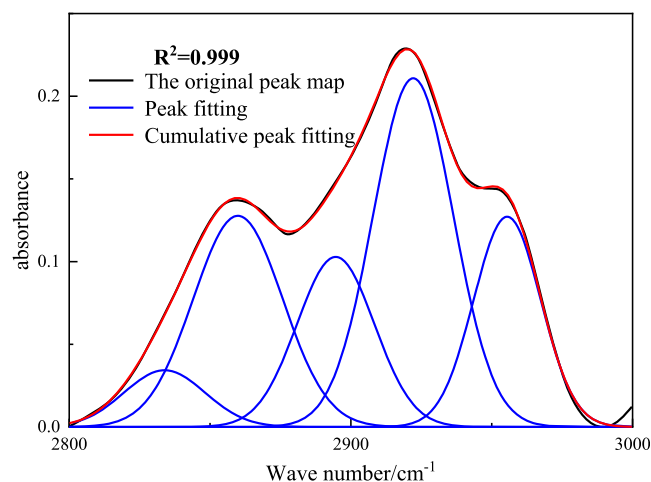


Figure 2. FT-IR fitting spectrum of the aliphatic hydrocarbon structure in coal.

Table 3. FT-IR Analysis Table of the Aliphatic Hydrocarbon Structure in Coal

spectral position attribution	peak type	peak weighted center (cm^{-1})	fwhm	peak area	peak area percentage (%)
asym. R_2CH_2	Gaussian	2833.85	33.84	1.22	5.79
sum. RCH_3	Gaussian	2859.89	37.41	5.08	24.03
R_3CH	Gaussian	2894.61	32.29	3.53	16.71
asym. R_2CH_2	Gaussian	2922.13	33.57	7.53	35.61
asym. RCH_3	Gaussian	2955.49	27.95	3.78	17.86

hydroxyl group formed on the aromatic ring is the most important hydroxyl structure of bituminous coal, accounting for 64.89%. This result indicates that the cyclization of the aliphatic chain in coal has a strong condensation effect with functional groups, which weakens the stretching vibration of free hydroxyl groups.

3.1.2. Aliphatic Hydrocarbon Structure. The aliphatic hydrocarbon structures in coal include chain aliphatic hydrocarbons and cyclic aliphatic hydrocarbons. There are five fitting characteristic peaks in the aliphatic hydrocarbon structure in

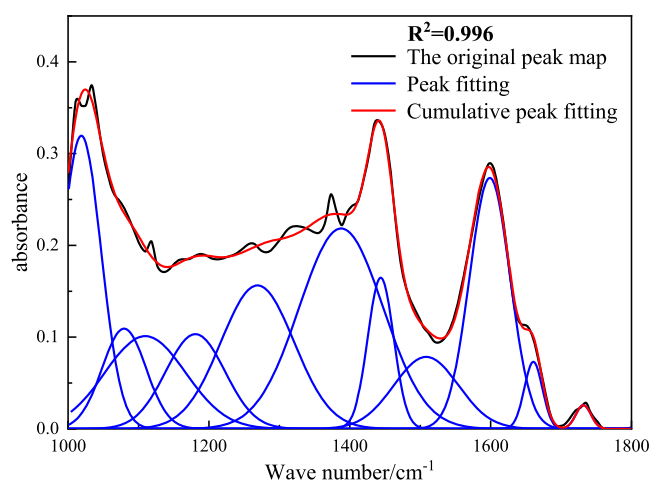


Figure 3. FT-IR fitting diagram of coal oxygen-containing functional groups.

Table 4. FT-IR Analysis Table of Oxygen-Containing Functional Groups in Coal

spectral position attribution	peak type	peak weighted center (cm ⁻¹)	fwhm	peak area	peak area percentage (%)
Si–O	Gaussian	1018.86	66.45	16.81	11.78
C–O	Gaussian	1079.56	73.48	8.49	5.96
C–O	Gaussian	1109.57	135.09	14.12	9.91
C–O	Gaussian	1180.77	99.21	10.91	7.64
C–O	Gaussian	1268.94	122.32	20.36	14.28
CH ₃ –Ar, R	Gaussian	1387.78	140.16	32.58	22.84
CH ₃	Gaussian	1443.93	43.23	7.58	5.31
C=C	Gaussian	1508.48	107.83	9.01	6.32
C=C	Gaussian	1598.83	67.75	19.72	13.83
C=O	Gaussian	1660.64	30.11	2.34	1.64
carboxyl acids	Gaussian	1731.69	25.14	0.69	0.49

Table 5. FT-IR Analysis Table of the Aromatic Hydrocarbon Structure in Coal

spectral position attribution	peak type	peak weighted center (cm ⁻¹)	fwhm	peak area	peak area percentage (%)
4H	Gaussian	743.65	20.61	1.21	12.26
4H	Gaussian	753.99	25.29	2.04	20.63
2H	Gaussian	803.54	38.42	3.75	37.95
1H	Gaussian	855.74	33.89	1.11	11.25
1H	Gaussian	871.62	26.29	1.77	17.91

bituminous coal, as shown in Figure 2. The relative contents of various structures are shown in Table 3.⁴¹

According to Table 3, in the absorption peak position range of 3000–2800 cm⁻¹, the five fitting peaks belong to the stretching vibrations of methyl groups, methylene groups, and methine groups. The proportion of methyl groups in aliphatic hydrocarbons is 41.89%. Methylene accounted for 41.40%, and methine accounted for 16.71%.

3.1.3. Oxygen-Containing Functional Groups. Bituminous coal has a strong silicon stretching vibration absorption peak at 1020–1030 cm⁻¹. To reduce interference, the fitting interval is adjusted to 1060–1800 cm⁻¹, and the fitted spectrum is shown in Figure 3. FT-IR fits of oxygen-containing functional groups generally have peaks of 13–18. In this study, 17 characteristic

peaks were fitted, and the fitting effect was ideal. The analytical results are shown in Table 4.⁴¹ The proportion of phenolic C–O and ether bonds in bituminous coal is 53.88%, the proportion of –CH₃ is 7.58%, and the proportion of carbonyl groups is 2.34%. These results show that the oxygen-containing functional groups of bituminous coal primarily exist in C–O bonds and aromatic rings.

3.1.4. Aromatic Hydrocarbon Structure. There are six characteristic peaks in the bituminous coal aromatic hydrocarbon structure (Table 5). The fitting spectrum is shown in Figure 2, and the peak structure attribution and relative content are shown in the table. According to Table 6,⁴¹ the aromatic hydrocarbon structure in bituminous coal primarily. The content of disubstituted benzene (2H) rings in bituminous coal was 37.95%, that of monosubstituted benzene (1H) rings was 29.16%, and that of tetra-substituted benzene (4H) rings was 32.89%. Disubstituted and trisubstituted substitutions in bituminous coal are the primary structures of coal molecules (Figure 4).

3.2. XPS Photoelectric Spectroscopy Analysis. The XPS energy spectrum test results of the bituminous coal samples are shown in Figure 5a. Different peak positions in the spectrum correspond to different element forms.

As shown in Figure 5b, the C spectrum is divided into four peak positions after fitting. The peak at 284.70 eV can be attributed to C–C and C–H, and the C structure accounts for 69.08%; the peak at 285.54 eV can be attributed to C–O in ether and hydroxyl groups, accounting for 21.09% in the C structure; the peak at 286.64 eV can be attributed to C=O in the carbonyl group, accounting for 4.62% in the C structure; and the peak at 289.46 eV can be attributed to COO– in the carboxyl group, which accounts for 5.21% of the C structure.⁴²

The O spectrum is shown in Figure 5c. After peak fitting, a total of three peak positions are divided. The peak at 530.9 eV can be attributed to carbonyl oxygen C=O, which accounts for 22.45% of the O structure. The peak at 532.11 eV can be attributed to the carbon–oxygen single bond C–O, accounting for 34.35% of the O structure; and the peak at 533.54 eV can be attributed to the carboxyl oxygen COO–, accounting for 43.20% of the O structure.⁴³

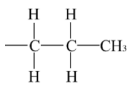
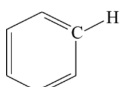
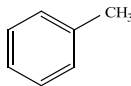
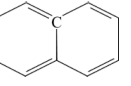
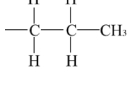
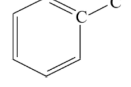
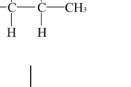
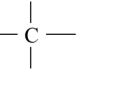
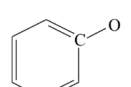
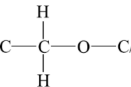
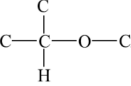
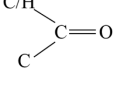
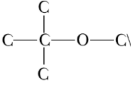
The N spectrum is shown in Figure 5d. A total of three peak positions are obtained after peak split fitting: the peak at 397.23 eV can be attributed to pyridine, and the proportion of the N structure is 15.88%; the peak at 400.21 eV can be attributed to pyrrole, which accounts for 25.29% of the N structure; and the peak at 401.62 eV can be attributed to quaternary nitrogen, which accounts for 58.83% of the N structure.⁴⁴

The S spectrum is shown in Figure 5e, and a total of three peak positions are obtained after subpeak fitting. The peak at 163.95 eV can be attributed to low-valent organic sulfide, which accounts for 40.55% of the S structure; the peak at 165.14 eV can be attributed to thiophenes, accounting for 32.49% of the S structure; and the peak at 169.34 eV can be attributed to inorganic sulfate, accounting for 26.96% of the S structure.¹⁹

3.3. ¹³C NMR Carbon Spectrum Analysis. **3.3.1. C NMR Carbon Spectrum Peak Division Analysis.** The chemical shift of ¹³C NMR is sensitive to the chemical environment and directly reflects the distribution of groups and electrons around the observed nucleus. The measured chemical shift range is generally 0–250 ppm, and Figures 6 and 7 show the ¹³C NMR characterization spectrum and the peak distribution spectrum.

Figure 6 shows that the ¹³C NMR spectrum can be roughly divided into five peaks based on chemical shifts: (1) aliphatic

Table 6. Structure Assignment of Chemical Shifts in ^{13}C NMR Spectra

Carbon structure name	Primary attribution	Typical chemical shift/ 10^{-6}	Carbon structure name	Primary attribution	Typical chemical shift/ 10^{-6}
Lipid methyl carbon		14-16	Protonated aromatic carbon		100-129
Aromatic methyl carbon		16-22	Bridgehead aromatic carbon		129-137
Mesomethylene carbon, Methylene carbon		22-36	Side branch aromatic carbon		137-148
Methylene carbon, Quarterly carbon	 	36-50	Oxygen substituted aromatic carbon		148-165
Oxygen methyl group and oxygen methylene carbon group.		50-56	Carbonyl carbon	—COOR/H	165-188
Oxymethylene carbon		60-70	Carbonyl carbons of aldehydes, quinones, phenyl ketones		188-205
Oxygen-grafted carbon		75-90	Carbonyl carbon of alkanone and cycloalkanone		205-220

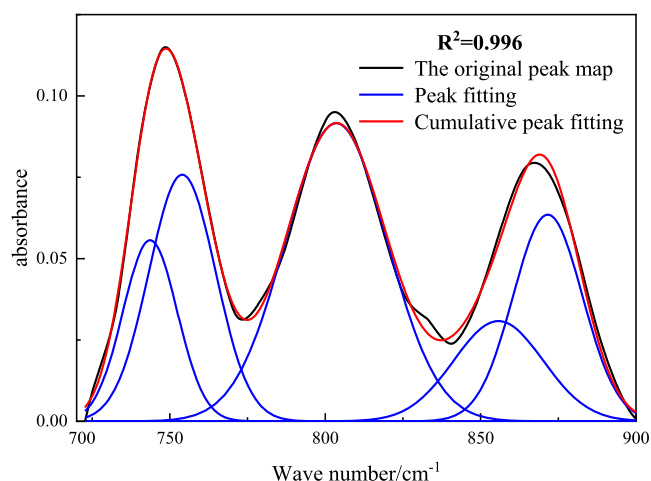


Figure 4. FT-IR fitting spectrum of the aromatic hydrocarbon structure in coal.

carbon peaks with chemical shifts of 0–60 ppm; (2) ether oxygen peaks with chemical shifts of 60–90 ppm; (3) chemical

shifts of 100–165 ppm for the aromatic carbon peak; (4) the carboxyl carbon peak with a chemical shift of 165–188 ppm; and (5) the carbonyl carbon peak with a chemical shift of approximately 188–220 ppm. The figure shows that two relatively high spectral peaks appear in the bituminous coal sample, and the chemical shifts in the range of 0–60 ppm are aliphatic and methine carbon structures. The chemical shifts are in the 100–165 ppm range for the structures of protonated aromatic carbons, bridgeheads, and side-branched aromatic carbons. The peak intensity at 100–165 ppm is much higher than that at 0–60 ppm. This result indicates that the aromatic organic molecular structure in the bituminous coal samples is the primary component, while the aliphatic methyl carbon and methine carbon are the secondary components. To facilitate the division of chemical structures at different shifts, the assigned structures of carbon chemical shifts of ^{13}C NMR are shown in Table 6.⁴⁵

The qualitative analysis of the structure of coal can provide information about the functional groups contained in the coal. If the structure must be characterized and determined, the content of each functional group must be quantitatively analyzed. Therefore, it is necessary to perform peak processing on ^{13}C

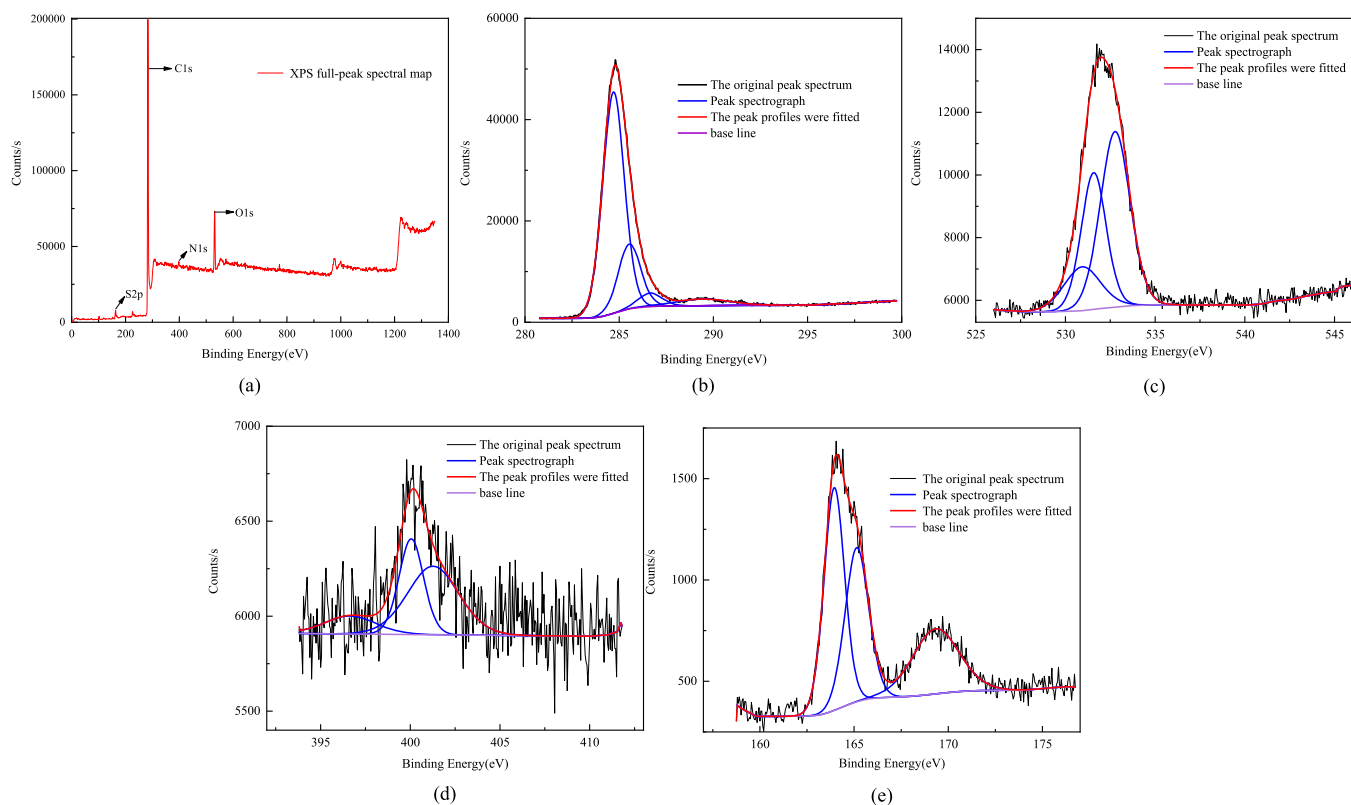


Figure 5. XPS detection spectrum and C, O, N, and S element peak fitting spectrum: (a) XPS full peak, (b) XPS C peak, (c) XPS O peak, (d) XPS N peak, and (e) XPS S peak.

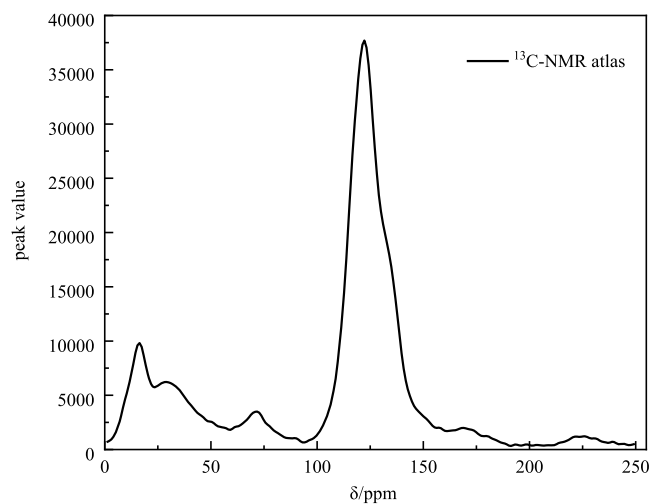


Figure 6. ^{13}C NMR spectrum of the coal sample.

NMR to determine the content and position of each functional group. Peakfit software was used to perform the peak fitting operation on the ^{13}C NMR data. Peak positions were added as completely as possible to ensure a higher degree of fit and accuracy, and the peak processing results agreed more with the experimental results. The carbon structure was assigned numerically (Table 2), and the proportion of the carbon skeleton structure and structural parameters were calculated by the relative area of the subpeaks.

The ^{13}C NMR test results of the carbon NMR spectrum of the bituminous coal sample show that the primary chemical shifts of the sample appear at $(0-70) \times 10^{-6}$, $(100-170) \times 10^{-6}$, and $(210-250) \times 10^{-6}$ places. After the peak split fitting operation, a

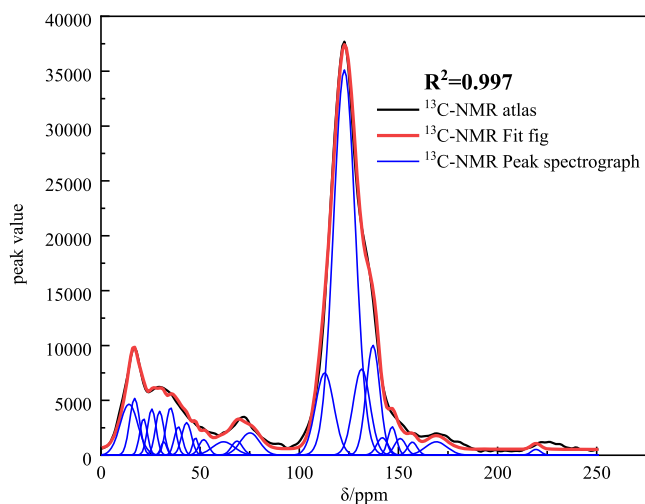


Figure 7. ^{13}C NMR peak fitting pattern of the coal sample.

total of 32 peak positions were added, and the fitting results fit the original spectrum, as shown in Figure 2. After calculating the relative area of each peak position and summarizing it, the proportion of protonated aromatic carbon in the coal sample is shown to be the highest, followed by bridgehead aromatic carbon, methylene carbon, and methine carbon. The carbonyl groups of aldehydes, quinones, and phenyl ketones account for 0.082%, which is negligible (Tables 7 and 8).

3.3.2. ^{13}C NMR Structure Analysis. To study the relative content of carbon atoms with different structures, Solum et al.⁴⁶ proposed 12 structural parameters of coal based on previous studies, including f_a (a total aromatic carbon rate), f_a^C (a

Table 7. Structure Attribution and Relative Area

structural attribution	structural proportions %
protonated aromatic carbon	22.161
bridgehead aromatic carbon	19.698
methylene carbon and methine carbon	19.255
methine carbon and quaternary carbon	11.987
side branch aromatic carbon	10.166
oxygen-substituted aromatic carbon	7.151
oxygen to methyl and oxygen to methylene carbon	4.697
aromatic methyl carbon	1.455
carbonyl carbon of alkanone and cycloalkanone	1.446
oxygen to methine carbon	1.130
aliphatic methyl carbon	0.771
carbonyl carbons of aldehydes, quinones, and phenyl ketones	0.082

carbonyl carbon rate), f_a' (a carbon rate in the aromatic ring), f_a^N (a protonated aromatic carbon rate), f_a^H (a protonated aromatic carbon rate), f_a^P (an oxygen-linked aromatic carbon rate), f_a^S (a side branch aromatic carbon rate), f_a^B (a bridged aromatic carbon rate), f_{al} (a total aliphatic carbon rate), f_{al}^* (a methyl carbon or quaternary carbon rate), f_{al}^H (a methylene or methine carbon rate), and f_{al}^O (an oxygenated aliphatic carbon rate).

In the complete structure, the sum of aromatic carbon and aliphatic carbon is 1. Based on the abovementioned parameters, the ratio of bridge carbon to peripheral carbon can be deduced to be

$$X_{BP} = \frac{f_a^B}{f_a^H + f_a^P + f_a^S} \quad (1)$$

Table 8. ^{13}C NMR Structural Parameters

f_a	f_a^C	f_a'	f_a^N	f_a^H	f_a^P	f_a^S	f_a^B	f_{al}	f_{al}^*	f_{al}^H	f_{al}^O
74.34	1.55	72.79	19.93	52.86	1.70	2.36	15.87	25.36	9.44	10.38	5.54

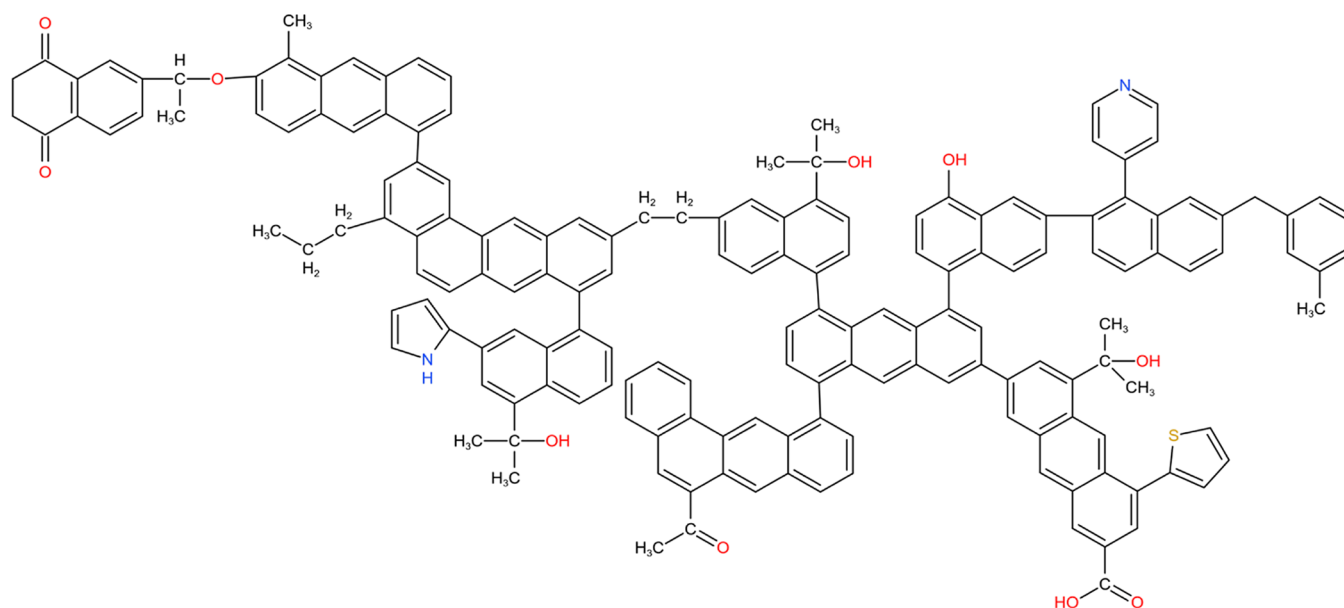


Figure 8. Planar model of the molecular structure of Baozigou coal.

This parameter describes the average value of the degree of condensation of aromatic rings in the coal structure, and the size of the aromatic clusters can be calculated.

The 12 structural parameter values of bituminous coal samples were obtained by calculating the data, and the X_{BP} value of the aromatic bridge carbon to weekly carbon ratio calculated by Formula 1 was 0.279. In the benzene ring structure, the X_{BP} value of benzene was 0, the X_{BP} value of naphthalene was 0.25, the X_{BP} value of anthracene was 0.4, the X_{BP} value of tetracene was 0.5, and the X_{BP} value of pentacene was 0.57. To control the molecular weight and reduce the computational complexity of the simulation, the structure ratio in the aromatic structure was adjusted and combined with the XPS data analysis results. The combination of four naphthalene, three anthracene, and two tetracene was finally determined. Aliphatic carbon structures exist in the form of methylene, methine, aliphatic side chains, and cycloalkanes. According to the analysis results of the carbon structure attribution in the table, the aliphatic carbons in this model were primarily methylene and methine carbons, while the proportion of aliphatic methyl carbons was nearly zero. The alkyl side chains were dominated by long-chain and naphthenic hydrocarbons. According to the analysis of the abovementioned experimental results, the total number of carbon atoms in the structural model was 150–170. According to the element content of the element industry analysis, the molecular structure plane unit model of bituminous coal was constructed. The plane unit model of the molecular structure of bituminous coal was drawn using kingdraw software and the molecular structure was $\text{C}_{169}\text{H}_{128}\text{O}_{10}\text{N}_2\text{S}$, as shown in Figure 8.

3.4. Model Validation of Coal. According to the joint analysis results of ^{13}C NMR, FT-IR, and XPS, the degree of polycondensation of benzene rings, the connection method of

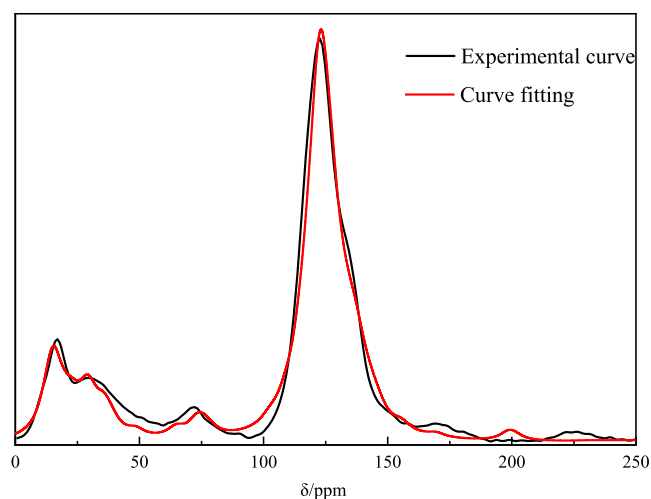


Figure 9. Simulation spectrum verification.

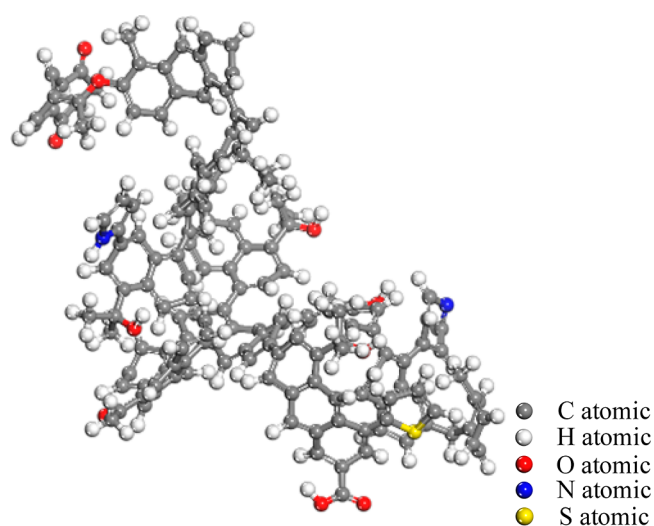


Figure 10. Molecular structure model of bituminous coal.

bridge carbon and the position of heteroatoms in the structure of different coal samples were determined. Combined with the elemental analysis of C, H, O, N, and S. The content of coal was preliminarily constructed. However, the constructed planar model may be different from the correct model due to the position of functional groups, and the initial model is continuously adjusted and optimized. This step was performed using ^{13}C spectral prediction in MestRenova software. The comparison between the final adjusted model and the original data model is shown in Figure 9.

3.5. Molecular Structure and Model Construction of Bituminous Coal Samples. The structure with the lowest energy in the simulation results was selected as the optimal geometry of the bituminous coal, as shown in Figure 10. After the optimization of molecular mechanics and molecular

Table 10. Pore Volume Parameters of Bituminous Coal Molecular Aggregates

occupied volume (\AA^3)	free volume (\AA^3)	surface area (\AA^2)
42025.14	6534.86	9985.43

dynamics, some chemical bonds, such as bridge bonds and aliphatic bonds, were twisted to achieve the minimum repulsion between functional groups in the single molecular structure. Because of the π - π interaction between the aromatic rings, the adjacent aromatic sheets tended to be arranged in parallel, and the interlayer spacing increased, exhibiting a 3D effect. Table 9 shows the energy composition of the bituminous coal structure model before and after optimization. The total energy was 6713.401 kJ/mol before optimization and 2667.595 kJ/mol after optimization, indicating a marked reduction in total energy. In the optimized model, the bond stretching energy and van der Waals energy decreased, other terms increased, and the total energy markedly decreased, indicating that the bond stretching energy and van der Waals energy were dominant in the structure, and the bond stretching energy belonged to valence electrons. The van der Waals energy is a nonbonding energy. Because coal is a macromolecular structure composed of multiple aromatic rings, the molecular model of bituminous coal was transformed in the simulation from a two-dimensional planar structure into a 3D structure. The energy and torsional energy increased and concurrently caused a reduction in the bond stretching potential energy. In the optimized 3D structure, the parallel arrangement of aromatic sheets produced a larger dispersion force, which was the primary reason for the observed decrease in van der Waals energy (Table 10).

3.6. Establishment of the Molecular Aggregation Structure Model of Bituminous Coal.

The aggregated structure model shows that the molecular structure is bent and twisted after optimization by molecular mechanics and molecular dynamics simulation. Because coal is an amorphous substance without long-range periodicity and restricted by surrounding molecules, the original approximate flat fragment carbon structure is twisted and deformed. Figure 11 shows that the molecular distribution of Baozigou coal is relatively uniform, and the oxygen-containing functional groups on the surface are uniformly distributed. The occupied volume of the coal was 42025.14 \AA^3 , the pore volume was 6534.86 \AA^3 (1.66 cc/g), and the surface area was 9985.43 \AA^2 , thus describing the structural characteristics of the Baozigou coal sample surface (Figure 12).

3.7. Analysis of Liquid Nitrogen Adsorption Experiment. The nitrogen adsorption and analytical curves of the coal samples are shown in Figure 11. When the relative pressure is 0.01–0.2, the adsorption capacity rises steadily, when the relative pressure is 0.2–0.8, the adsorption capacity rises relatively gently, and when the relative pressure is 0.8–0.995, the adsorption capacity increases more obviously. When the relative pressure was 0.995, the maximum adsorption amount was 1.68 cc/g . The difference from the constructed model is 0.02 cc/g , which proves the accuracy of the model establishment.

Table 9. Energy Composition of the Bituminous Coal Structure Model

state	total energy	valence energy			nonbond energy		
		bond	angle	torsion	inversion	van der Waals	electrostatic
initial	6713.401	1225.408	308.759	3106.939	131.147	1343.187	−93.181
finally	2667.595	56.135	112.354	2643.820	48.999	103.501	−173.839

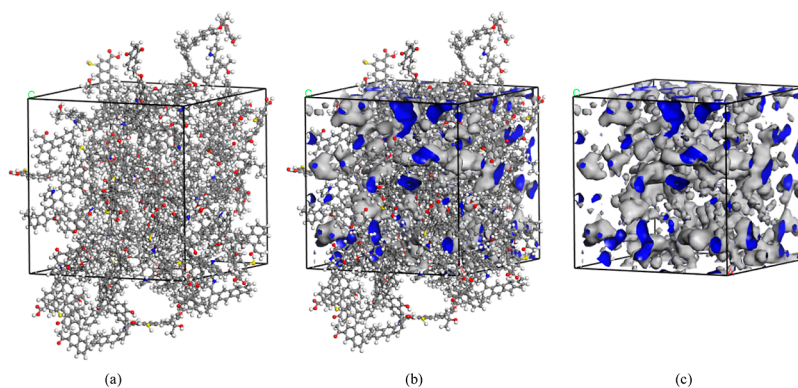


Figure 11. Molecular aggregation state model and pore distribution of bituminous coal: (a) agglomeration model of coal, (b) aggregate state model and pore volume of coal, and (c) pore volume of coal.

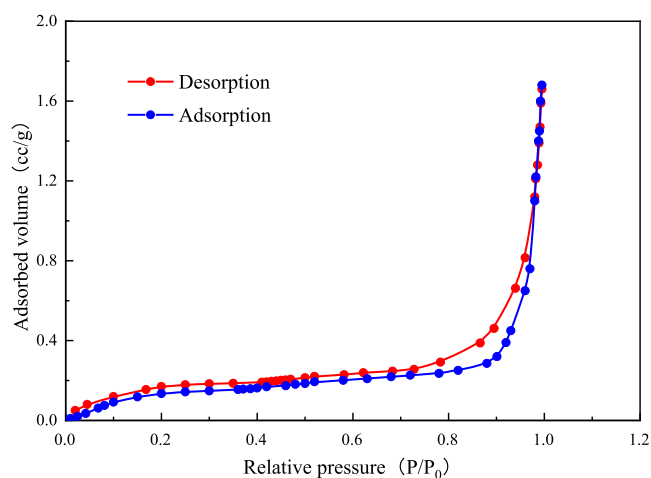


Figure 12. Nitrogen adsorption and analytical curves.

4. CONCLUSIONS

- (1) According to ^{13}C NMR, 12 structural parameters of the Baozigou bituminous coal structure were obtained, and the ratio of aromatic bridge carbon to peripheral carbon in the molecular structure of the coal was calculated to be 0.279. The combined test results of ^{13}C NMR, XPS, and FT-IR showed that bituminous coal's carbon atoms in the coal sample are primarily aromatic carbon structures. The aromatic structural units in the coal sample include four naphthalene, three anthracenes, and two tetracene. The heteroatoms in the coal molecular structure are three carbonyls, where one exists as phenolic hydroxyl, one pyrrole, and one pyridine. The final constructed bituminous coal had a molecular formula of $\text{C}_{169}\text{H}_{128}\text{O}_{10}\text{N}_2\text{S}$ and a molecular weight of 2378.
- (2) After geometric optimization and molecular dynamics simulation of a single molecular structure model using Materials Studio software, chemical bonds such as bridge bonds and aliphatic bonds were found to be twisted, and the π - π interaction between the aromatic sheets in the molecule made the adjacent aromatic sheets. The lamellae tended to be approximately parallel to each other. The total molecular energy before and after optimization decreased from 6713.401 to 2667.595 kJ/mol, and bond stretching energy and van der Waals energy dominated.

- (3) The aggregated structure model of 20 bituminous coal molecules was constructed. After optimization by molecular mechanics and molecular dynamics simulations, the macromolecules in the aggregated structure model were restricted by surrounding molecules, and the original sheet-like aromatic carbon structure was approximately parallel. Distortion occurred, the lamellar structure was disordered, and the complete condensed matter structure model was compact. The coal had an occupied volume of 42025.14 \AA^3 , a pore volume of 6534.86 \AA^3 , and a surface area of 9985.43 \AA^2 . When the relative pressure of liquid nitrogen is 0.995, the adsorption capacity is 1.68 cc/g, which is 0.02 cc/g different from the established model, which verifies the accuracy of the model.

AUTHOR INFORMATION

Corresponding Authors

Deji Jing – College of Safety Science and Engineering, Liaoning Technical University, Fuxin 123000, China; Key Laboratory of Mine Thermodynamic Disaster and Control of Ministry of Education, Fuxin 123000, China; Email: jingdeji@163.com

Xiangxi Meng – College of Safety Science and Engineering, Liaoning Technical University, Fuxin 123000, China; Key Laboratory of Mine Thermodynamic Disaster and Control of Ministry of Education, Fuxin 123000, China; orcid.org/0000-0002-5570-0288; Email: 455062996@qq.com

Authors

Shaocheng Ge – College of Safety and Emergency Management Engineering, Taiyuan 030024, China; orcid.org/0000-0001-7398-9102

Tian Zhang – College of Safety Science and Engineering, Liaoning Technical University, Fuxin 123000, China; Key Laboratory of Mine Thermodynamic Disaster and Control of Ministry of Education, Fuxin 123000, China; orcid.org/0000-0002-9739-2711

Mingxing Ma – College of Safety Science and Engineering, Liaoning Technical University, Fuxin 123000, China; Key Laboratory of Mine Thermodynamic Disaster and Control of Ministry of Education, Fuxin 123000, China

Gang Wang – CCTEG Shenyang Research Institute, Fushun 123000, China

Complete contact information is available at:
<https://pubs.acs.org/10.1021/acsomega.2c00505>

Author Contributions

¹X.M. are contributed equally to this work.

Notes

The authors declare no competing financial interest.

ACKNOWLEDGMENTS

This work was financially supported by the National Natural Science Foundation of China (no. 51704146); the Natural Science Foundation of Liaoning Province (no. 2020-MS-304); and the Scientific Research Fund of Liaoning Provincial Education Department (no. LJKZ0323).

REFERENCES

- (1) Jing, D.; Jia, X.; Ge, S.; Zhang, T.; Ma, M. Numerical simulation and experimental study of vortex blowing suction dust control in a coal yard with multiple dust production points. *Powder Technol.* **2021**, *388*, 554–565.
- (2) Jing, D.; Meng, X.; Ge, S.; Zhang, T.; Ma, M.; Tong, L. Reconstruction and seepage simulation of a coal pore-fracture network based on CT technology. *PLoS One* **2021**, *16*, No. e0252277.
- (3) Tian, Z.; Deji, J.; Shaocheng, G.; Wang, J.; Meng, X. Numerical simulation of the dimensional transformation of atomization in a supersonic aerodynamic atomization dust-removing nozzle based on transonic speed compressible flow. *Int. J. Coal Sci. Technol.* **2020**, *7*, 597–610.
- (4) Han, S.; Chen, H.; Harvey, M. A.; Stemm, E. Focusing on Coal Workers' Lung Diseases: A Comparative Analysis of China, Australia, and the United States. *Int. Res. J. Publ. Environ. Health* **2018**, *15*, 1–26.
- (5) Yang, S.; Nie, W.; Lv, S.; Liu, Z.; Peng, H.; Ma, X. Effects of spraying pressure and installation angle of nozzles on atomization characteristics of external spraying system at a fully-mechanized mining face. *Powder Technol.* **2019**, *343*, 754–764.
- (6) Hua, Y.; Nie, W.; Liu, Q.; Peng, H.; Wei, W.; Cai, P. The development and application of a novel multi-radial-vortex-based ventilation system for dust removal in a fully mechanized tunnelling face. *Tunn. Undergr. Space Technol.* **2020**, *98*, 103253.
- (7) Ma, Q.; Nie, W.; Yang, C.; Peng, H.; Liu, Z.; Guo, C.; Cai, X. Effect of spraying on coal dust diffusion in a coal mine based on a numerical simulation. *Environ. Pollut.* **2020**, *264*, 114717.
- (8) Xue, Q.; Nie, W.; Guo, L.; Liu, Q.; Sun, N.; Liu, C. Determining the optimal airflow rate to minimize air pollution in tunnels. *Process Saf. Environ. Prot.* **2021**, *157*, 115–130.
- (9) Liu, S.; Liu, X.; Guo, Z.; Liu, Y.; Guo, J.; Zhang, S. Wettability modification and restraint of moisture re-adsorption of lignite using cationic gemini surfactant. *Colloid. Surface.* **2016**, *508*, 286–293.
- (10) Chen, S.; Tao, X.; He, H.; Chen, L.; Yang, Z. Enhancing flotation performance of low rank coal by improving its hydrophobicity and the property of oily bubbles using 2-ethylhexanol. *Int. J. Miner. Process.* **2017**, *167*, 61–67.
- (11) Xia, Y.; Zhang, R.; Xing, Y.; Gui, X. Improving the adsorption of oily collector on the surface of low-rank coal during flotation using a cationic surfactant: An experimental and molecular dynamics simulation study. *Fuel* **2019**, *235*, 687–695.
- (12) Paajanen, A.; Vaari, J. High-temperature decomposition of the cellulose molecule: a stochastic molecular dynamics study. *Cellulose* **2017**, *24*, 2713–2725.
- (13) Xu, Y.; Liu, Y.-L.; Gao, S.; Jiang, Z.-W.; Su, D.; Liu, G.-S. Monolayer adsorption of dodecylamine Surfactants at the mica/water interface. *Chem. Eng. Sci.* **2014**, *114*, 58–69.
- (14) Yan, F.; Xu, J.; Peng, S.; Zou, Q.; Li, Q.; Long, K.; Zhao, Z. Effect of capacitance on physicochemical evolution characteristics of bituminous coal treated by high-voltage electric pulses. *Powder Technol.* **2020**, *367*, 47–55.
- (15) Xia, Y.; Yang, Z.; Zhang, R.; Xing, Y.; Gui, X. Enhancement of the surface hydrophobicity of low-rank coal by adsorbing DTAB: An experimental and molecular dynamics simulation study. *Fuel* **2019**, *239*, 145–152.
- (16) Hu, Y.; Zhang, Q.; Zhou, G.; Wang, H.; Bai, Y.; Liu, Y. Influence Mechanism of Surfactants on Wettability of Coal with Different Metamorphic Degrees Based on Infrared Spectrum Experiments. *ACS Omega* **2021**, *6*, 22248–22258.
- (17) Xu, F.; Liu, H.; Wang, Q.; Pan, S.; Zhao, D.; Liu, Y. Study of non-isothermal pyrolysis mechanism of lignite using ReaxFF molecular dynamics simulations. *Fuel* **2019**, *256*, 115884.
- (18) Wang, C.; Watson, J. K.; Louw, E.; Mathews, J. P. A construction strategy for atomistic models of coal chars capturing stacking diversity and pore size distribution. *Energy Fuels* **2015**, *29*, 4814–4826.
- (19) An, P.; Xia, W.; Peng, Y.; Xie, G. Construction of bituminous coal vitrinite and inertinite molecular assisted by ¹³C NMR, FTIR and XPS. *J. Mol. Struct.* **2020**, *1222*, 128959.
- (20) Lin, H.; Wang, Y.; Gao, S.; Xue, Y.; Yan, C.; Han, S. Chemical structural characteristics of high inertinite coal. *Fuel* **2021**, *286*, 119283.
- (21) Wang, J.; Tian, L.; Li, G.; Zhao, X.; Liang, Y.; Yu, J. Construction of vitrinite molecular structures based on ¹³C NMR and FT-IR analysis: Fundamental insight into coal thermoplastic properties. *Fuel* **2021**, *300*, 120981.
- (22) He, X.; Liu, X.; Nie, B.; Song, D. FTIR and Raman spectroscopy characterization of functional groups in various rank coals. *Fuel* **2017**, *206*, 555–563.
- (23) Wang, H.; Liu, S.; Li, X.; Yang, D.; Wang, X.; Song, C. Morphological and structural evolution of bituminous coal slime particles during the process of combustion. *Fuel* **2018**, *218*, 49–58.
- (24) Xiang, J.; Zeng, F.; Bin, L.; Zhang, L.; Li, M.-f.; Liang, H.-z. Construction of macromolecular structural model of anthracite from Chengzhuang coal mine and its molecular simulation. *J. Fuel Chem. Technol.* **2013**, *41*, 391–400.
- (25) Pan, J.; Zhu, H.; Hou, Q.; Wang, H.; Wang, S. Macromolecular and pore structures of Chinese tectonically deformed coal studied by atomic force microscopy. *Fuel* **2015**, *139*, 94–101.
- (26) Lian, J.; Lin, H.; Xue, Y.; Sheng, H. Study on the structural differences between Heidaigou long flame coal and its vitrinite. *Energy Sources Part A* **2019**, *41*, 78–85.
- (27) Fu, Y.; Liu, X.; Ge, B.; Liu, Z. Role of chemical structures in coalbed methane adsorption for anthracites and bituminous coals. *Adsorption* **2017**, *23*, 711–721.
- (28) Kozłowski, M. XPS study of reductively and non-reductively modified coals. *Fuel* **2004**, *83*, 259–265.
- (29) Jiang, J.; Weihua, Y.; Yuanping, C. Molecular structure characterization of middle-high rank coal via XRD, Raman and FT-IR spectroscopy: implications for coalification. *Fuel* **2019**, *239*, 559–572.
- (30) Lin, H.; Lian, J.; Liu, Y.; Xue, Y.; Yan, S.; Han, S.; Wei, W. Comprehensive study of structure model, pyrolysis and liquefaction behaviour of Heidaigou lignite and its liquefied oil. *Fuel* **2019**, *240*, 84–91.
- (31) Liu, Z.; Gang, Z.; Shuailong, L. Molecular dynamics simulation and experimental characterization of anionic surfactant: Influence on wettability of low-rank coal. *Fuel* **2020**, *279*, 118323.
- (32) Xia, Y.; Rui, Z.; Yaowen, X. Improving the adsorption of oily collector on the surface of low-rank coal during flotation using a cationic surfactant: An experimental and molecular dynamics simulation study. *Fuel* **2019**, *235*, 687–695.
- (33) Meng, J.; Feifei, Y.; Shichao, L. Effect of different concentrations of surfactant on the wettability of coal by molecular dynamics simulation. *Int. J. Min. Sci. Technol.* **2019**, *29*, 577–584.
- (34) Lyu, X.; Xiaofang, Y.; Meng, H. Adsorption and molecular dynamics simulations of nonionic surfactant on the low rank coal surface. *Fuel* **2018**, *211*, 529–534.
- (35) Hou, Y.; Yang, F.; Yang, C.; Feng, Z.; Feng, L.; Li, H.; Ren, S.; Wu, W. A study on the structure of anthracite based on benzene carboxylic acids. *J. Energy Inst.* **2021**, *98*, 153–160.
- (36) Yang, F.; Wu, W.; Wang, Q.; Niu, M.; Ren, S. The relationship between benzene carboxylic acids from coal via selective oxidation and coal rank. *Fuel Process. Technol.* **2017**, *160*, 207–215.
- (37) Zhou, J.; Wang, Y.; Huang, X. Determination of O-containing functional groups distribution in low-rank coals by chemical titration. *J. Fuel Chem. Technol.* **2013**, *41*, 134–138.

- (38) Zhang, X.; Kang, T.; Zhang, B.; Kang, G.; Kang, J.; Zhang, R.; Zhang, L. Combined Molecular Simulations and Experimental Study of Methane Adsorption on Anthracite. *Energy Fuels* **2020**, *34*, 12118–12125.
- (39) Mathews, J. P.; Sharma, A. The structural alignment of coal and the analogous case of Argonne Upper Freeport coal. *Fuel* **2012**, *95*, 19–24.
- (40) Solomon, P. R.; Carangelo, R. M. FTIR analysis of coal. I. Techniques and determination of hydroxyl concentrations. *Fuel* **1982**, *61*, 663–669.
- (41) Ibarra, J. V.; Muñoz, E.; Rafael, M. FTIR study of the evolution of coal structure during the coalification process. *Org. Geochem.* **1996**, *24*, 725–735.
- (42) Perry, D. L.; Grint, A. Application of XPS to coal characterization. *Fuel* **1983**, *62*, 1024–1033.
- (43) Xu, C.; Zhou, G.; Qiu, H. Analysis of the microscopic mechanism of coal wettability evolution in different metamorphic states based on NMR and XPS experiments. *RSC Adv.* **2017**, *7*, 47954–47965.
- (44) Kelemen, S. R.; Gorbaty, M. L.; Kwiatek, P. J. Quantification of Nitrogen Forms in Argonne Premium Coals. *Energy Fuels* **1994**, *8*, 896–906.
- (45) Zoran, T.; Srejac, R.; Vucelic, D.; Vitorovic, D.; Jovancicevic, B. Structural analysis of Aleksinac oil shale kerogen by high-resolution solid-state ^{13}C nmr, spectroscopy. *Fuel* **1995**, *74*, 1903–1909.
- (46) Solum, M. S.; Pugmire, R. J.; Grant, D. M.; Kelemen, S. R.; Gorbaty, M. L.; Wind, R. A. N-15 CP-MAS NMR of the argonne premium coals. *Energy Fuels* **1997**, *11*, 491–494.